9-20-2021

Following the Lithium: Tracing Li-bearing Molecules across Age, Mass, and Gravity in Brown Dwarfs

Ehsan Gharib-Nezhad

Mark S. Marley

Natasha E. Batalha

Channon Visscher

Richard S. Freedman

See next page for additional authors

Following the Lithium: Tracing Li-bearing Molecules across Age, Mass, and Gravity in Brown Dwarfs

Abstract

Lithium is an important element for the understanding of ultracool dwarfs because it is lost to fusion at masses above ∼68 MJ. Hence, the presence of atomic Li has served as an indicator of the nearby H-burning boundary at about 75 MJ between brown dwarfs and very low mass stars. Historically, the "lithium test," a search for the presence of the Li line at 670.8 nm, has been a marker if an object has a substellar mass. While the Li test could, in principle, be used to distinguish masses of later-type L–T dwarfs, Li is predominantly no longer found as an atomic gas but rather a molecular species such as LiH, LiF, LiOH, and LiCl in cooler atmospheres. The L- and T-type dwarfs are quite faint at 670 nm and thus challenging targets for high-resolution spectroscopy. But only recently have experimental molecular line lists become available for the molecular Li species, allowing molecular Li mass discrimination. Here we generated the latest opacity of these Li-bearing molecules and performed a thermochemical equilibrium atmospheric composition calculation of their abundances. Finally, we computed thermal emission spectra for a series of radiative–convective equilibrium models of cloudy and cloudless brown dwarf atmospheres (with Teff = 500–2400 K and log 4.0 5.0 g = –) to understand where the presence of atmospheric lithium-bearing species is most easily detected as a function of brown dwarf mass and age. After atomic Li, the best spectral signatures were found to be LiF at 10.5–12.5 μm and LiCl at 14.5–18.5 μm. Also, LiH shows a narrow feature at ∼9.38 μm.

Keywords

brown dwarfs, L dwarfs, T dwarfs, T subdwarfs, spectral line lists

Disciplines

Stars, Interstellar Medium and the Galaxy

Authors

Ehsan Gharib-Nezhad, Mark S. Marley, Natasha E. Batalha, Channon Visscher, Richard S. Freedman, and Roxana E. Lupu

The Astrophysical Journal, 919:21 (9pp), 2021 September 20 https://doi.org/10.3847/1538-4357/ac0a7d

Following the Lithium: Tracing Li-bearing Molecules across Age, Mass, and Gravity in Brown Dwarfs

Ehsan Gharib-Nezhad[1,7], Mark S. Marley[2], Natasha E. Batalha[1], Channon Visscher[3,4], Richard S. Freedman[1,5], and Roxana E. Lupu[6]
[1] NASA Ames Research Center, Moffett Field, CA 94035, USA
[2] Lunar and Planetary Laboratory, University of Arizona, Tucson, AZ 85721, USA
[3] Chemistry & Planetary Sciences, Dordt University, Sioux Center, IA 51250, USA
[4] Center for Extrasolar Planetary Systems, Space Science Institute, Boulder, CO 80301, USA
[5] SETI Institute, Mountain View, CA 94035, USA
[6] BAER Institute/NASA Ames Research Center, Moffett Field, CA 94035, USA
Received 2021 March 26; revised 2021 June 1; accepted 2021 June 3; published 2021 September 17

Abstract

Lithium is an important element for the understanding of ultracool dwarfs because it is lost to fusion at masses above $\sim$68 M_J. Hence, the presence of atomic Li has served as an indicator of the nearby H-burning boundary at about 75 M_J between brown dwarfs and very low mass stars. Historically, the "lithium test," a search for the presence of the Li line at 670.8 nm, has been a marker if an object has a substellar mass. While the Li test could, in principle, be used to distinguish masses of later-type L–T dwarfs, Li is predominantly no longer found as an atomic gas but rather a molecular species such as LiH, LiF, LiOH, and LiCl in cooler atmospheres. The L- and T-type dwarfs are quite faint at 670 nm and thus challenging targets for high-resolution spectroscopy. But only recently have experimental molecular line lists become available for the molecular Li species, allowing molecular Li mass discrimination. Here we generated the latest opacity of these Li-bearing molecules and performed a thermochemical equilibrium atmospheric composition calculation of their abundances. Finally, we computed thermal emission spectra for a series of radiative–convective equilibrium models of cloudy and cloudless brown dwarf atmospheres (with $T_{\rm eff} = 500$–2400 K and $\log g = 4.0$–5.0) to understand where the presence of atmospheric lithium-bearing species is most easily detected as a function of brown dwarf mass and age. After atomic Li, the best spectral signatures were found to be LiF at 10.5–12.5 μm and LiCl at 14.5–18.5 μm. Also, LiH shows a narrow feature at $\sim$9.38 μm.

Unified Astronomy Thesaurus concepts: Brown dwarfs (185); L dwarfs (894); T dwarfs (1679); T subdwarfs (1680); Spectral line lists (2082)

1. Introduction

More than 25 yr ago, the observation of the first brown dwarfs, Teide 1 and Gliese 229B, ushered in a new era in astronomy (Nakajima et al. 1995; Oppenheimer et al. 1995; Rebolo et al. 1995). Since then, many models and observations have been done to understand the chemistry and physics of brown dwarf atmospheres; their atmospheric evolution with age, mass, and effective temperature (e.g., Burrows et al. 1997; Chabrier et al. 2000; Saumon & Marley 2008); and their connection to the planet and stellar main characteristics (e.g., Marley & Robinson 2015; Zhang 2020). Luminosity, age, mass, radius, surface gravity, atmospheric evolution, effective temperature, and cloud/aerosol formation are among the main active open questions waiting to be addressed to better understand these objects.

One indicator used to distinguish between stars and brown dwarfs is the detection of the atomic lithium resonance line at 670.8 nm, which was proposed by Rebolo et al. (1992) and aptly named the "lithium test." Atomic Li is converted to He through fusion at central temperatures of $\sim(2$–$3) \times 10^6$ K. Thus, objects that are not massive enough to reach such temperatures in their interior do not burn Li (Pozio 1991). Nelson et al. (1993) calculated a transition mass of 62–65 M_J for the Li burning. Magazzu et al. (1993) showed that the required mass to burn Li by half is $M = 84$ and 63 M_J for 60 and 250 Myr objects, respectively. Similarly, Chabrier et al. (1996) modeled the depletion of Li along with mass and age and found that the initial lithium burns by a factor of 2 over $\sim$0.26 Gyr and a factor of 100 over $\sim$1 Gyr for a 64 M_J object. In addition, Bildsten et al. (1997) provided an analytical formation to calculate the Li depletion as a function of age, mass, radius, and luminosity of objects within 52–105 M_J. By comparison, current calculations place the mass limit for H burning at 74 M_J (e.g., Marley et al. 2021). Because of the happy near-coincidence of these two masses, the detection of Li has become a straightforward diagnostic test of most brown dwarfs, even though consumption of Li in the most massive brown dwarfs leads to their confusion with the lowest-mass stars (Basri 2000).

Interestingly, Rebolo et al. (1996) further validated Teide 1 as a true brown dwarf through the detection of atomic lithium and application of the lithium test. Since then, several studies have implemented the Li test to confirm the true detection of brown dwarfs and also determine their ages and masses (e.g., Martín et al. 1999). Age is difficult to ascertain, however, and systematic studies of the Li strength of a sample of $\sim$150 late M to L dwarfs by Kirkpatrick et al. (2008) did not reveal any strong correlation with age.

In general, the Li test has been challenging to apply to all types of brown dwarfs. First, moderately large telescopes are required with a resolution $\lambda/\Delta\lambda \geqslant 1200$ and signal-to-noise ratio (S/N) of $\sim$50 to detect the Li resonance line at 670.8 nm

[7] NASA Postdoctoral Fellow.

(Martín et al. 1999; Kirkpatrick et al. 2008).[8] Second, for the mass interval between this minimum Li-burning mass and the hydrogen-burning minimum mass, $\sim 74\,M_{\rm J}$, absent atomic lithium is ambiguous as a star/brown dwarf discriminant. This is particularly troublesome in the effective temperature range occupied by both young massive brown dwarfs and the coolest, lowest-mass stars.

For objects cooler than any star at the bottom of the main sequence, there is no question that an object is substellar (e.g., the atmospheric methane detected in Gl 229B clearly indicated a substellar atmosphere; Oppenheimer et al. 1995). However, the Li test still has relevance even at these cool effective temperatures. Gravity signatures for brown dwarfs are currently lacking, and beyond general rules of thumb, such as the triangular-shaped H band as a signpost of low gravity in L dwarfs (Kirkpatrick et al. 2008), there are no straightforward markers of mass in brown dwarfs. As a result, many L- and T-type dwarfs have uncertain masses. This is primarily due to the well-known degeneracy between age, mass, and gravity.

Specific examples of objects with divergent mass estimates include Gliese 229B (late T, ~1000 K), for which Brandt et al. (2020), by combining radial velocities, imaging, and astrometry methods, derived a dynamical mass of $\sim 70 \pm 5\ M_{\rm J}$, whereas early evolutionary models suggested a younger age and noticeably lower mass of 20–55 $M_{\rm J}$ (Allard et al. 1996; Marley et al. 1996). The T dwarf HD 19467B is another object (T5–T7, ~1050 K) with high uncertainty in its modeled mass and age, which are $74^{+12}_{-9} M_{\rm J}$ and ~9–11 Gyr (Maire et al. 2020). Another T dwarf example is GJ 570D (T7.5, ~800 K) with a calculated mass of 15–72 $M_{\rm J}$ (Geballe et al. 2001). This degeneracy problem is not only limited to T dwarfs. Objects HD 7672B and HD 4747B are two examples of massive L dwarfs (L4.5 and L8, ~1700 K) with large uncertainties in their mass and age (Liu et al. 2002; Crepp et al. 2016). For objects such as these, a discrete mass discriminant would be particularly valuable.

Note that the computed thermal evolution tracks of brown dwarfs (e.g., Marley et al. 2021) predict that objects massive enough to burn Li would not cool below 900 K in the age of the universe. However, as some of the above mass estimates attest, a few objects, like Gl 229B, have reported apparently problematic masses. Having an independent mass indicator would greatly illuminate such cases.

To the best of our knowledge, there has been only one study before by Weck et al. (2004) to investigate the LiCl signature for dwarfs with $T_{\rm eff} = 900$–1500 K. However, the main goals of their study were to provide the LiCl ab initio line list and consider the brown dwarf effective temperature range over which LiCl could be detected. In comparison, we here assess a broader range of atmospheric temperatures and include all Li species for which there are opacity data available.

We have organized this article as follows. In Section 2, we give an account of the equilibrium chemistry in M to T dwarfs, and the chemistry of the dominant Li-bearing molecules is explained. In Section 3, we describe the calculation of absorption cross-section (ACS; or opacity) data for LiH, LiF, and LiCl molecules. The degeneracy in the determination of brown dwarf masses is addressed in Section 4. Following that, Section 5 presents a set of synthetic thermal fluxes for brown dwarfs with effective temperatures in the range of 500–2400 K and for surface gravity ($\log g$) of 4.0, 4.5, and 5.0. In this section, the presence and spectral location of LiH, LiF, and LiCl molecules in the cloudy and clear atmospheres is discussed. In the end, Section 5.3 comments on the nondetection of atomic Li in T dwarf observed fluxes even if modeling spectra predict its presence. A summary and future works are presented in Section 6.

[8] Note that a lower S/N and resolution is required to record the Li resonance line in L dwarfs. For example, Martín et al. (2018) showed that S/N > 15 and $\lambda/\Delta\lambda \geqslant 600$ are sufficient to detect the Li 6708 Å absorption in L-type Hyades brown dwarf candidates.

2. Lithium Chemistry

Thermochemical equilibrium simulations are performed to calculate the abundance of the following species in the temperature–pressure space at 75–6000 K and 10^{-6}–3000 bars: Li(g), LiOH, LiH, LiF, LiCl, e^-, H_2, H, H^+, H^-, H_2^-, H_2^+, H_3^+, H_2O, CH_4, C_2H_2, C_2H_4, C_2H_6, CO, CO_2, NH_3, N_2, HCN, OCS, PH_3, H_2S, TiO, VO, FeH, CrH, SiO, MgH, He, Na, K, Rb, Cs, Fe, graphite, Li(s), Li2S(s), LiF(s), and LiCl(s). Since we are exploring objects in which lithium is not expected to burn, we used the protosolar abundance of Li in this study. We adopt the protosolar Li abundance from Lodders (2003; i.e., A(Li) = 3.28), which is derived from meteoritic CI chondrites (carbonaceous meteorites of Ivuna type). The CI chondrites are the most primitive chondrites because they have not chemically fractionated, and their relative abundances are considered to be similar to the protosolar abundance. Therefore, they are enriched in elements like lithium.

Figure 1 illustrates the volume mixing ratios (VMRs) of Li-bearing species predicted by equilibrium chemistry as a function of temperature (left) and pressure (right). There are three main thermal regions in the VMR–T–P parameter space as defined by these species. The first is hot atmospheres with $T_{\rm eff}$ of ~1800–2800 K (e.g., M–L dwarfs) in which monoatomic Li is the dominant gas in $\sim 10^{-3}$–100 bars. The second is warm atmospheres with $T_{\rm eff}$ of ~900–1800 K (e.g., L–T dwarfs) where LiCl and LiOH dominate. The third region, with $T_{\rm eff} \leqslant 1000$, is characterized by LiF and LiCl as the favored molecules.

Figure 2 illustrates a broad view of the presence and abundance of Li species in the temperature–pressure space. In this phase diagram, Li, LiCl, LiOH, and LiF are shown by yellow, green, blue, and red shading. For example, gaseous Li is the most stable form at $T > 1400$ K. At each area, dashed and dotted contour lines represent 50% and 20% of that species with respect to the total protosolar lithium abundance ($\sim 3.5 \times 10^{-9}$) in the atmosphere. The solid and dashed black curves are the $T(P)$ profiles (for $\log g = 5$) for cloudy and cloudless (Marley et al. 2021) models, respectively. We aim to understand whether these different Li species domains can be recognized in brown dwarf spectra and if they could serve as mass indicators.

3. Absorption Cross Sections

Radiative transfer modeling of synthetic thermal emission requires accurate and complete ACS data of Li(g), LiH, LiF, and LiCl. The ACS data of a given absorber consists of several million lines with a unique position, intensity, and width. The width is sensitive to the temperature and pressure of broadening gases, and it is controlled by the convolution of Doppler and Lorentz profiles. The knowledge of pressure-broadening coefficients for the Lorentz profile is instrumental and

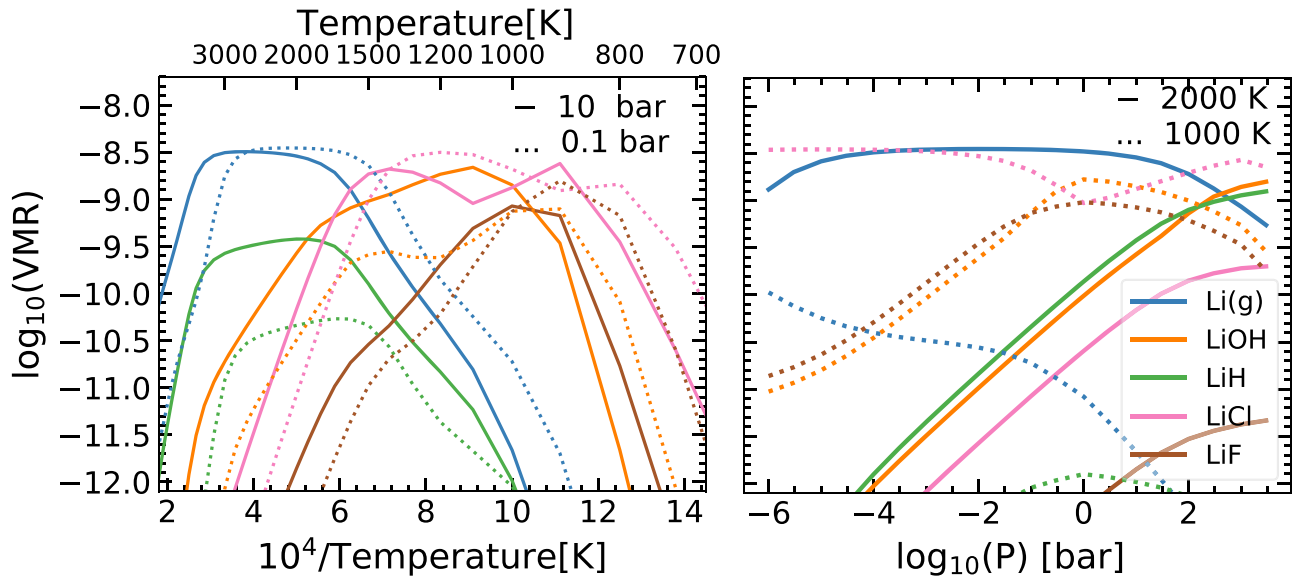

Figure 1. Volume mixing ratio (VMR) plots of Li(g), LiF, LiCl, LiH, and LiOH with respect to temperature (left) and pressure (right). At high temperatures ($T \gtrsim 1500$ K), gaseous Li is the most abundant Li-bearing species. At moderate temperatures (1500 K $\lesssim T \lesssim$ 1000 K), both LiCl and LiOH will be the most stable form of Li-bearing species, depending on the pressure. At low pressures and low temperatures ($P \lesssim 0.01$ bar and $T \lesssim 1000$ K), LiF could also be abundant.

dependent on J quantum numbers. The choice of broadening for the background gases in this study is 85% H_2 and 15% He by number. Because the H_2 and He pressure-broadening Lorentz coefficients for these species have not been calculated or measured, we have estimated the pressure-broadening data for the Li-broadening molecules in question.

In a recent paper (Gharib-Nezhad et al. 2021), we provided a detailed discussion on how to generate these ACS data and their pressure-broadening coefficients. The generated ACS data of atomic Li(g), LiH, LiF, and LiCl cover 1460 temperature and pressure grid points and a range of 75–4000 K and 10^{-6}–3000 bars, respectively. The line lists used to generate these ACS data are the most accurate and up-to-date and provided in Table 1. Note that the LiOH line list is not available; hence, we could not generate the LiOH ACS data. The pregenerated ACS data of LiH, LiF, and LiCl from this study are publicly available in 10.5281/zenodo.4921928.

Figure 3 depicts the weighted ACS × VMR for Li, LiH, LiF, and LiCl for 800, 1600, and 2600 K at $P = 10$ bars. The dominant spectral features LiH, LiF, and LiCl are approximately located at ∼9–10, 10.5–14, and 14.5–19 μm, respectively. Although the atomic Li is not favored at $T < 1000$ K, its ACS value is a few orders of magnitude greater than its molecular forms. Hence, the Li absorption is predominant in the optical region and, as we will show, is present even after molecular species become predominant in cooler atmospheric layers. At $T < 2000$ K, LiCl and LiF become predominant features in the infrared.

4. Degeneracy on Age–Mass–Gravity Space: Challenges

Figure 4 presents in black the Sonora-Bobcat solar-metallicity evolution tracks for isolated 10–83 M_J dwarfs in $\log g - T_{\rm eff}$ parameter space from Marley et al. (2021). Green curves show isochrones from 0.04 to 10 Gyr. This figure also shows the Li depletion region (yellow), where atomic Li is depleted by fusion. The presence and overlap of LiF, LiCl, and LiH molecules are highlighted as well.

Our understanding of brown dwarfs is shaped by the degeneracy in the $T_{\rm eff} - t - g - M - R - L$ space (i.e., effective temperature, age, surface gravity, mass, radius, luminosity). The $T_{\rm eff}$ and L parameters may be estimated from observational spectra (e.g., Cushing et al. 2005; Saumon & Marley 2008). In addition, objects with masses 20–80 M_J and age $\geqslant$0.2 Gyr have radii within a range of 0.7–1.3 R_J (e.g., see Figure 3 by Burrows et al. 2001). As a result, age, gravity, and mass are the three puzzling parameters, as younger, lower-mass objects can have comparable luminosity and spectra to older, higher-mass objects.

There have been attempts to disentangle this $M - t - g$ degeneracy by employing atomic and molecular spectral features as a probe. For instance, McGovern et al. (2004) proposed estimating the gravity and age by comparing the absorption features of Na I, K I, Cs I, Rb I, TiO, VO, CaH, and FeH at ∼0.7–1.25 μm. Following that, Kirkpatrick et al. (2008) used the strength and the presence or absence of gravity-sensitive features of Na I, K I, CaH, the TiO/VO ratio, and H_α emission to determine the youth and gravity of a large sample of late M–L dwarfs. Allers & Liu (2013) also used FeH, VO, K I, and the H-band continuum shape to probe the gravity of several ultracool M5–L7 dwarfs.

5. Modeling M–L–T Dwarf Atmospheres: Cloudy and Clear

In this work, we aim to explore the utility of the Li-bearing species to help disentangle age, mass, and gravity in brown dwarfs by providing a well-defined mass boundary. Figure 4 highlights which Li species would denote which regions and where the absence of Li would signify a high mass. Details of the evolutionary and atmospheric models are provided in Section 5.1, followed by discussion of the results in Sections 5.2 and 5.3.

5.1. Modeling Details

Here we utilize the Sonora-Bobcat generation of atmosphere models computed for brown dwarfs with clear atmospheres by

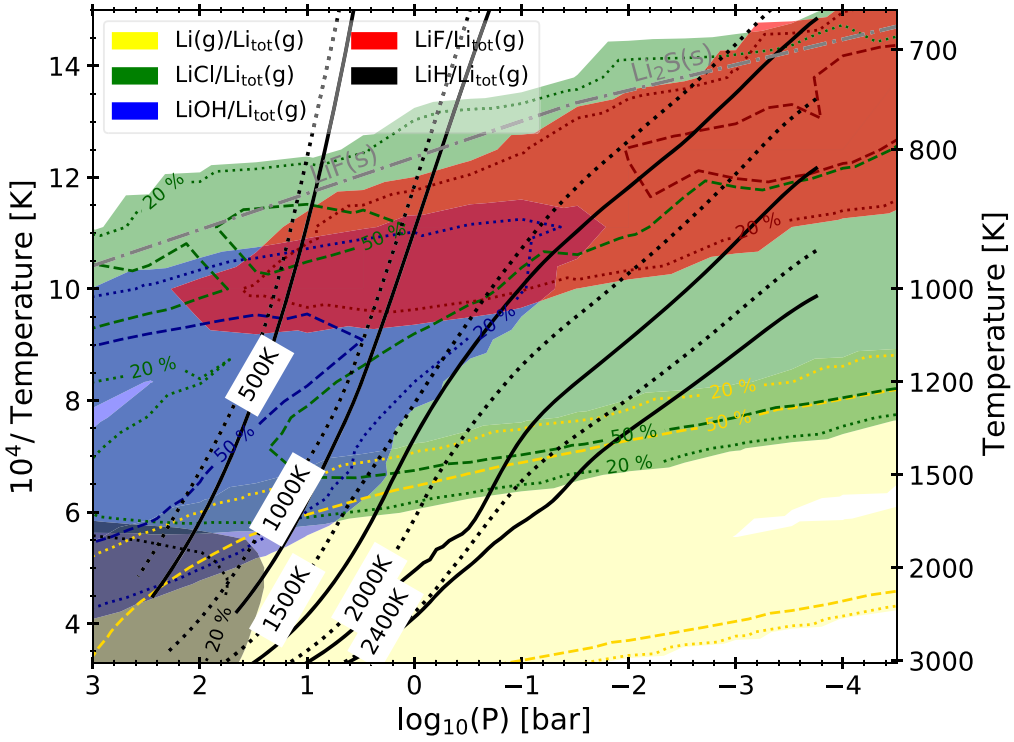

Figure 2. Li phase diagram: temperature–pressure diagram showing the mole fraction of atomic gaseous Li (yellow), LiH (black), LiOH (blue), LiCl (green), and LiF (red). For each area, the dotted and dashed contours represent the 20% and 50% of the species with respect to the total Lithium abundance in both solid and gas phases (i.e., the protosolar value $\sim 3.5 \times 10^{-9}$). The solid and dashed black curves are the $T(P)$ profiles (for $\log g = 5$) for cloudy and cloudless (Marley et al. 2021) models, respectively. As a brown dwarf cools, the dominant Li-bearing species in the observable atmosphere (generally $P < 10$ bar) varies.

Table 1
Summary List of Opacities: Molecules, Temperature, Pressures, and Their Line Lists

Absorber	λ [μm]	Method	Reference
LiCl	2.2–330	laboratory	(Bittner & Bernath 2018)
LiF	5.5–330	laboratory	(Bittner & Bernath 2018)
LiH	5.5–330	ab initio	(Coppola et al. 2011)

Note. We computed the ACS over the pressure and temperature ranges of 10^{-6}–3000 bar and 75–4000 K. See Section 3 for more details.

Marley et al. (2021). These are supplemented by a few additional cloudy models computed specifically for this study, following the same methodology and cloud treatment described in Ackerman & Marley (2001). For each model of interest, we compute a high-resolution spectrum using `PICASO`, an open-source radiative transfer code (Batalha 2019; Batalha et al. 2019).[9]

We used our generated opacities for Li(g), LiH, LiCl, and LiF, as well as opacities from Freedman et al. (2014; see Table 2 in Lupu et al. 2014, for details) for other species mentioned in Section 2. We did not investigate LiOH due to the lack of a line list, although theoretical ab initio studies suggest that the LiOH main rotation–vibration bands are located at 2.6, 10.8, and 31.3 μm (e.g., Bunker et al. 1989; Koput 2013). The evolution calculation is from Marley et al. (2021).

[9] https://natashabatalha.github.io/picaso/

5.2. Impact of Li, LiCl, LiF, and LiH on Brown Dwarf Spectra

We investigate the influence of Li species on the emergent spectra of candidate brown dwarfs with protosolar abundances. We consider effective temperatures ($T_{\rm eff}$) of 500, 1000, 1500, 2000, and 2400 K and $\log g = 4.0$, 4.5, and 5 to span the range of conditions of interest where Li species may be detected. The cloudy models are computed for this study for all of the aforementioned $T_{\rm eff}$ but with $f_{\rm sed} = 3$ and $\log g = 5$. The sedimentation parameter, $f_{\rm sed}$, controls the particle size and vertical extent of the cloud layer (Ackerman & Marley 2001). Aluminum oxide (Al2O3), forsterite (Mg_2SiO_4(s)), and Fe(l,s)) cloud species are included. The location of the modeled objects on the evolutionary model space is indicated with yellow circles in Figure 4.

The presence, absence, and strength of the Li species spectral features on emergent spectra are assessed for different effective temperatures and surface gravities to see if they can productively be used as a high-mass indicator in brown dwarfs. For each case, we perform the model twice by in turn including (ON) and excluding (OFF) each molecule or atom in our calculation of the emergent thermal spectrum. This was done to isolate the effect of each species. The results for cloudy and cloudless models are illustrated in Figures 5 (for $\log g = 5$) and 6 (for $\log g = 4.0$, 4.5, and 5). In Figure 5, the top panels represent the 500–2400 K synthetic thermal fluxes with Li, LiH, LiF, and LiCl ON (solid) and OFF (dashed). The bottom panels show the relative flux ratio, which is the difference between $F^{\rm ON}$ and $F^{\rm OFF}$ normalized by $F^{\rm OFF}$ (hereafter $\mathcal{F}_{\rm R} \equiv \frac{F^{\rm OFF} - F^{\rm ON}}{F^{\rm OFF}}$). In Figure 6, $\log g = 4.0$, 4.5, and 5 are shown with dashed-dotted, dotted, and dashed lines, respectively, which includes both ON and OFF cases.

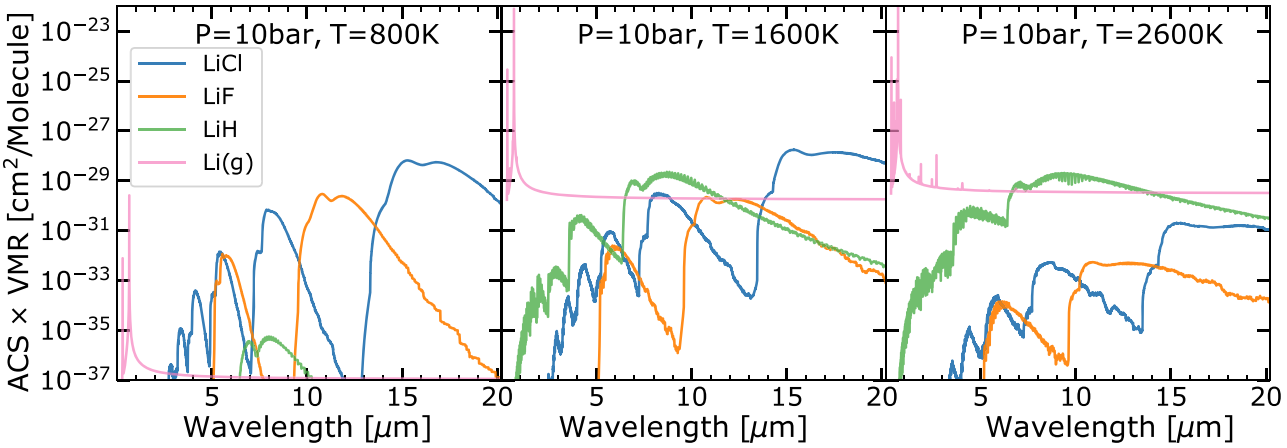

Figure 3. Smoothed absorption cross-sections (ACSs) of atomic Li, LiH, LiF, and LiCl multiplied by its volume mixing ratios (VMR) for $P = 10$ bar. The resonance Li line at 670.8 nm has a large ACS value than its other molecular forms, and so its ACS × VMR value is larger than others even at low temperatures. In contrast, LiCl and LiF are the two dominant molecules at low temperatures and their spectral features are clearly distinguishable. At 1600 K, the fundamental band of LiH at ∼8.5 μm is dominant. In this study, their latest line lists are used to compute their opacities and also their pressure-broadening coefficients are revised. See Table 1 for more details.

Our focus is to ascertain whether the presence or absence of each Li species under different atmospheric effective temperatures and gravities can be detected in the synthetic emergent spectra. Below, we discuss each species in turn in order to better interpret these spectra and how they relate to the object's mass.

Atomic Li is the predominant form of Li species at high temperatures. The Li resonance line is shown in the left panel of Figure 1 at 0.667–0.675 μm. Since Li has a large opacity (see Figure 3), its absorption is predicted even at $T_{\rm eff} < 1000$ K in both cloudy and cloudless models. Given the fact that Li absorption is narrow and in a faint part of the spectrum, it requires a resolution of $R \geqslant 1200$ and S/N of >50 to be detected (Martín et al. 1999; Kirkpatrick et al. 2008). In particular, for T dwarfs, large telescopes and a significant amount of exposure time are required.

In the cloudy model (Figure 5), the Li $\mathcal{F}_{\rm R}^{Li}$ ratio has the largest value, which is ∼100% at the line center for $T_{\rm eff} = 1500$ K. In contrast, this ratio decreases to ∼20% for $T_{\rm eff} = 500$ K, and this might be why Li has not been observed in late-type T dwarfs (see Section 5.3 for more details). Note that this Li $\mathcal{F}_{\rm R}$ ratio is about 3–4 orders of magnitude larger than LiH, LiF, and LiCl, which shows the significant difference between the presence and absence of atomic Li in the model spectra.

In the clear model (Figure 6), the Li $\mathcal{F}_{\rm R}$ ratio for $T_{\rm eff} = 1500$–2000 K is 100% for all surface gravities ($\log g = 4.0$, 4.5, 5) at the line center. The behavior of the $\mathcal{F}_{\rm R}^{\rm Li}$ value with the wavelength in the wings (i.e., $d\mathcal{F}_{\rm R}^{\rm Li}/d\lambda$) could also be an indicator of the gravity because $d\mathcal{F}_{\rm R}^{\rm Li}/d\lambda$ is larger for $T_{\rm eff} = 2400$ and 500 K in models with smaller surface gravity. Comparing the $\log g$ of 4.0, 4.5, and 5 in Figure 6 shows the negligible impact that surface gravity has on the Li line core. This change in the wings with surface gravity appears in the figure.

Comparing cloudy and clear models for Li shows some remarkable changes in the Li $F^{\rm OFF}$ and $F^{\rm ON}$ fluxes and slightly in the $\mathcal{F}_{\rm R}^{\rm Li}$ ratio. Clouds have the largest impact on atmospheres with $T_{\rm eff}$ of 1000–2000 K, although the cloudy models still exhibit the atomic Li line.

The molecular form of Li at high temperatures is LiH, and its spectral feature is located at 7–10 μm, but its $\mathcal{F}_{\rm R}^{\rm LiH}$ ratio is greatest at ∼9.36 μm, according to our results. The $\mathcal{F}_{\rm R}$ ratio at $T_{\rm eff} > 1000$ K is ∼0.001%–0.005%, which would be challenging to detect. In the cloudy model, the highest $\mathcal{F}_{\rm R}^{\rm LiH}$ ratio is for $T_{\rm eff} = 1500$ K, while this changes to 2000 K for the clear model. Assessing both cloud and cloudless models and different surface gravities suggests that LiH is not sensitive to gravity and so could not be employed as a gravity indicator. However, the LiH region (black area) in Figure 4 shows that its detection can be an indicator of $M < 65\ M_{\rm J}$ and a temperature of ∼1700–2500 K. Moreover, LiH is present in young objects with $t < 1.0$ Gyr.

The LiF absorption feature is most prominent in the spectral range of 10.5–12.5 μm. As predicted by thermochemical equilibrium, LiF mostly forms at ∼800–1200 K, and its $\mathcal{F}_{\rm R}^{\rm LiF}$ ratio is almost ∼0.005%–0.5% for T–L dwarfs with $T_{\rm eff}$ of 900–1600 K. According to the cloudy and clear models, LiF can only be detected in atmospheres with $T_{\rm eff}$ in 1000–1500 K. In the clear model, $\log g = 4.0$ has the greatest $\mathcal{F}_{\rm R}^{\rm LiF}$. According to the evolutionary $T_{\rm eff} - g - t - M$ parameter space (Figure 4), the detection of LiF is a signature of an object with $M \leqslant 65\ M_{\rm J}$ and $t \leqslant 10$ Gyr. Lower surface gravity in this space leads to a higher $\mathcal{F}_{\rm R}^{\rm LiF}$ ratio and hence lower mass and younger age.

The predominant LiCl feature is located at 14.5–18.5 μm. This molecule is present for $T_{\rm eff} = 1000$–2100 K, and its $\mathcal{F}_{\rm R}^{\rm LiCl}$ ratio is ∼0.005%–0.5%. The feature is most detectable at $T_{\rm eff} = 1500$–2100 K. Both cloudy and clear models show that the LiCl feature and its $\mathcal{F}_{\rm R}^{\rm LiCl}$ ratio are sensitive to surface gravity. The $\mathcal{F}_{\rm R}^{\rm LiCl}$ is strongest for the lowest-gravity case considered, $\log g = 4.0$. Such objects would be young and low mass (i.e., $M \leqslant 15\ M_{\rm J}$ and $t \leqslant 0.1$ Gyr). The LiCl is less detectable in higher-gravity objects. Figure 4 illustrates the relation between the detection of these species and mass, gravity, and age. Note that both LiCl and LiF features are present in the range $T_{\rm eff} = \sim 900$–1600 K, and their $\mathcal{F}_{\rm R}$ ratio is higher for objects with lower surface gravity.

Weck et al. (2004) investigated the signature of LiCl on dwarfs with $T_{\rm eff} = 900$–1500 K and $\log g = 3.0$, 4.0, and 5.0 using the PHOENIX code with solar abundance. They

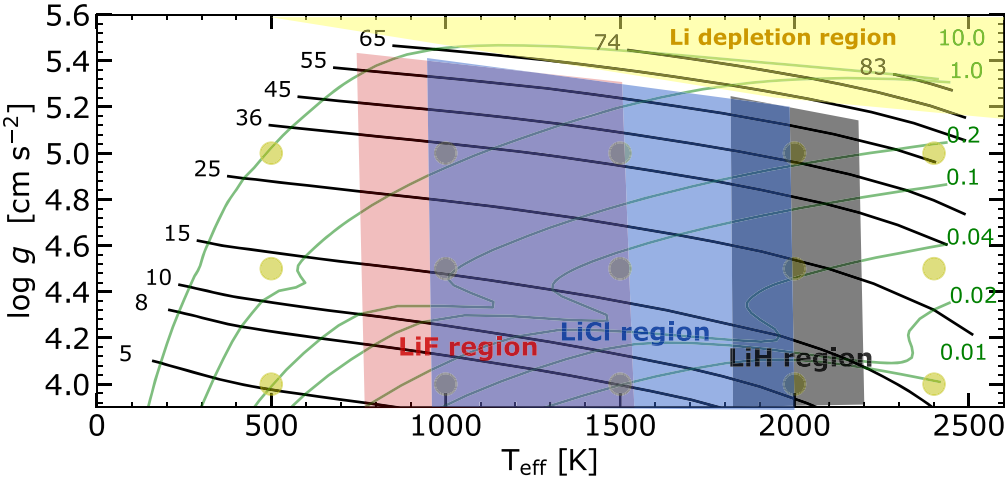

Figure 4. Evolution tracks (black, moving right to left with increasing age) showing gravity as a function of effective temperature for substellar-mass objects. Masses (black, in M_J) and ages (green, in Gyr) are labeled. Yellow circles denote individual radiative–convective models shown in the other figures ($T_{\rm eff}$ = 500, 1000, 1500, 2000, 2400 K, and surface gravity of $\log g$ = 4.0, 4.5 and 5.0 for cloudless models. The Sonora-Bobcat evolution grid models are adopted from Marley et al. (2021). Objects in the yellow area are massive and old enough to burn protosolar Li atoms. LiH, LiCl, and LiF spectral features become apparent in the black, blue, and red areas, respectively. For the strength of their features, see Figures 5–6.

concluded that the strongest $\mathcal{F}_R$ LiCl features are expected in T dwarfs with $T_{\rm eff} = 1200$ K and $\log g = 3.0$. According to the evolutionary models, only very young objects with ages <0.01 Gyr and masses <10 M_J could have $T_{\rm eff} = 1200$ K and $\log g = 3.0$. In comparison to their work, our main focus here is to study all Li species but for older objects with greater surface gravity and so with greater mass (i.e., 5 $M_J \leqslant M \leqslant 65$ M_J). We also assess the impact of clouds on the detection of the various Li species using the latest and most accurate opacity data.

In another study, Pavlenko et al. (2007) calculated the atomic Li resonance abundance in the LP 944-20 M dwarf atmosphere using VLT/UVES and AAT/SPIRAL observed spectra. They used DUSTY and COND model atmospheres from Allard et al. (2001) with solar metallicity; included Li, LiOH, LiH, LiF, LiBr, and LiCl species; and obtained $\log N({\rm Li}) = 3.25 \pm 0.25$. They found that atomic Li is the predominant Li-bearing species in objects with $T_{\rm eff} = 1800$–2400 K with $\log g = 4.5$.

5.3. Comments on Atomic Li Line in T Dwarfs

Figure 7 presents a set of observed emergent spectra for different T dwarfs, encompassing Gliese 570D (T8), 2MASS 1503+2525 (T5.5; Burgasser et al. 2003b), and 2MASS 0755+2212 (T5; Burgasser et al. 2002). These T dwarfs apparently do not show any atomic Li absorption in their spectra. In this figure, SDSS 0423–0414 (SDSS J042348.57–041403.5) is obtained from Kirkpatrick et al. (2008) and is the only object in these spectra that shows Li absorption with a pseudoequivalent width measurement of 11 Å. Note that this object is a peculiar one because its optical part is classified as L7.5, while the near-infrared part is T0 (Vrba et al. 2004). We also showed our synthetic spectra from the clear (dotted) and cloudy (dashed) models to highlight the presence of atomic Li from our modeling work.

The key difference between the observed and modeled spectra is the atomic Li line at 6708 Å. At low temperatures, atmospheric thermodynamic simulations expect Li to predominantly be found in the atomic form only at high P (see Figure 1 in Lodders 1999). Nevertheless, our grids of atmospheric cloudy and clear models predict the presence of the atomic Li line even at $T_{\rm eff} \simeq 600$ K (e.g., Allard et al. 2001; Burrows et al. 2002). However, the observed T dwarf spectra do not show any sign of Li detection at $T_{\rm eff} \leqslant 900$ K (e.g., Kirkpatrick et al. 2000; Burgasser et al. 2003a). Theoretically, this cannot simply be due to lithium burning having removed Li, as objects massive enough to burn Li are not expected to cool below 900 K in the age of the universe (e.g., Marley et al. 2021), although the dynamical masses for at least some T dwarfs come close (e.g., Brandt et al. 2020; Sahlmann et al. 2020).

Other possible explanations for the predicted atomic Li not being found in the data include incorrect Li thermochemistry data and clouds obscuring the deeper, higher-pressure regions where atomic Li resides. The accuracy of thermochemical data for key reactions such as LiOH+H = Li+H_2O and LiH +H = Li, as well as the impact of condensation on the abundance of Li gas, needs further investigation. Greater cloud opacity in the optical than considered here might also obscure the Li line. Additionally, since this Li line is located in the faint part of the optical spectrum, higher-S/N spectra should be acquired to more robustly test if the feature is indeed missing. The detection of Li at 670.8 nm at $T_{\rm eff} < 1000$ K deserves further observational and theoretical attention.

6. Conclusion and Future Work

Since the discovery of the first brown dwarfs, numerous massive cool dwarfs have been detected. However, ascertaining precise masses has been a challenge to the degeneracy between mass, gravity, and age for these objects. Therefore, the calculated mass of many ultracool dwarfs, including Gl 229B and Gl 510D, is still under debate and spans a wide range.

Traditionally, the Li test has been used to distinguish between low-mass stars and brown dwarfs with similar spectral types. At lower temperatures, such as L–T dwarfs, LiF and LiCl molecules form. Because LiF and LiCl features are located in regions where brown dwarfs are brighter than 670 nm, they could, in principle, be used as mass indicators at these lower effective temperatures.

In this paper, we investigated the spectral signatures of LiCl, LiF, and LiH, as well as atomic Li, using cloudy and cloudless

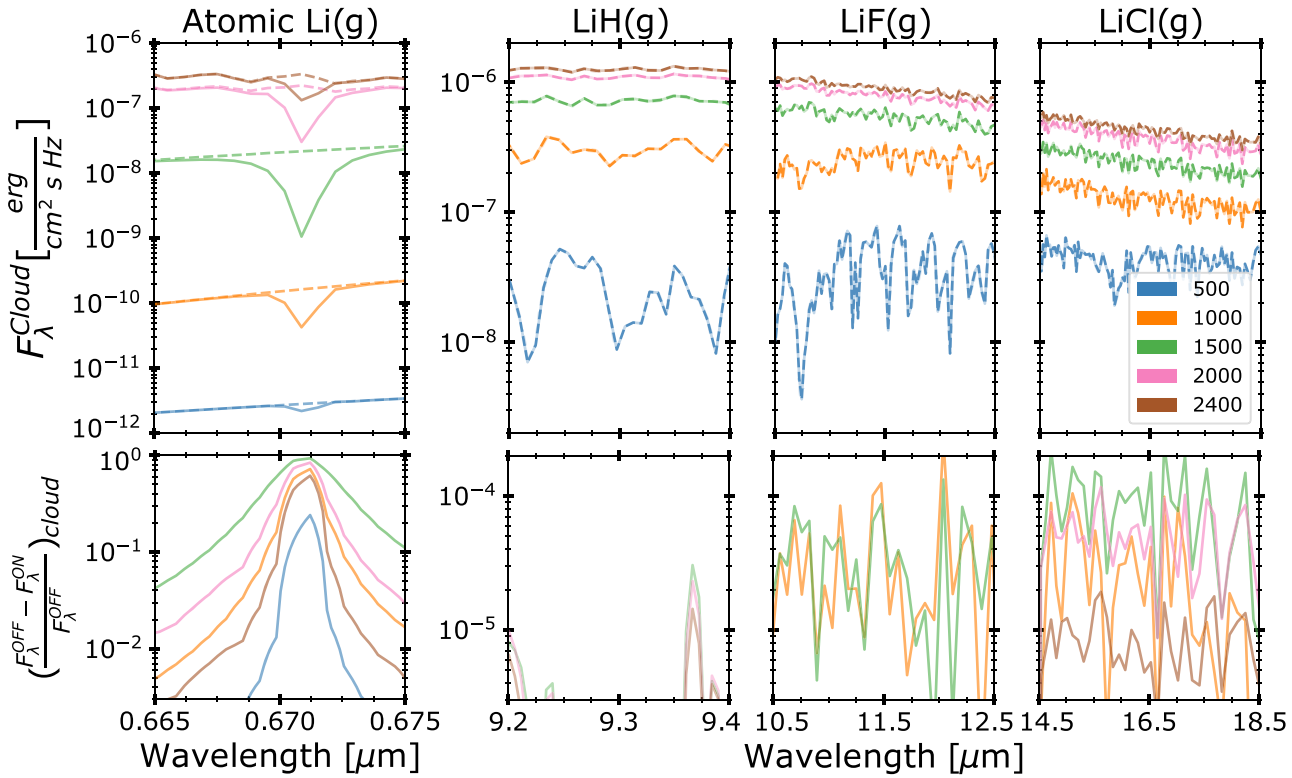

Figure 5. Overview of model spectra as computed for cloudy models with various $T_{\rm eff}$ in 500–2400 K range with $\log g = 5.0$ and $f_{\rm sed} = 3$. The top row of panels shows the computed spectra as computed with ($F^{\rm ON}$, solid) and without ($F^{\rm OFF}$, dashed) Li, LiH, LiF, and LiCl. Note the difference in the vertical axis between Li and the other species; in contrast to Li-bearing molecules, atomic Li shows an easily apparent difference between its $F^{\rm ON}$ and $F^{\rm OFF}$ fluxes. The lower row of panels shows the relative flux ratio, which is the difference between $F^{\rm ON}$ and $F^{\rm OFF}$ normalized by $F^{\rm OFF}$ ($\mathcal{F}_{\rm R} \equiv \frac{F^{\rm OFF}-F^{\rm ON}}{F^{\rm OFF}}$). All spectra are smoothed for clarity. LiF and LiCl could be an indicator of dwarfs with $M < 65 M_{\rm J}$ at $T_{\rm eff}$ ranges of 1000–1500 K and 1000–2000 K, respectively. Their absence in the observational spectra would be an indicator of higher mass.

atmospheric models. We showed that LiCl is present at an effective temperature of ∼1000–2000 K in cloudy atmospheres and ∼1500–2000 K in clear atmospheres. Hence, the LiCl spectral features should be found in L–T dwarfs with masses below 65 $M_{\rm J}$. The lack of LiCl at these $T_{\rm eff}$ would be an indicator of larger masses with concomitant older ages and larger surface gravities. The LiF feature at 10.5–12.5 μm is another indicator of masses lower than 65 $M_{\rm J}$ and $T_{\rm eff} \leqslant 1600$ K. The LiH is a stable molecule at high temperatures (e.g., early L–M dwarfs); however, its signature is confined to a narrow spectral interval of 9.35–9.4 μm. We could not assess the contribution of LiOH because of the lack of appropriate opacity data. In ultracool T dwarfs, such as Gl 229B, with a large mass uncertainty, the detection of LiF and LiCl would confirm that the object has a mass lower than 68 $M_{\rm J}$.

The relative flux ratio, $\mathcal{F}_{\rm R}$, of LiF and LiCl is very small; thus, the detection of these species requires high-S/N spectra in the mid-IR. However, their strongest spectral bands are found in the relatively bright region of the infrared thermal with less overlap with other spectral features than the atomic Li line in the optical, making them potentially favorable mass indicators. The James Webb Space Telescope MIRI instrument covers the wavelength range of 5–28 μm, and its spectrograph will enable medium-resolution spectroscopy with $\lambda/\Delta\lambda \sim 2000$–3700, so MIRI might be capable of detecting these Li features.

The high-resolution cross-correlation technique could be another method to detect LiH, LiF, and LiCl molecules. In this method, the number of detected lines is crucial to increasing the S/N, so a large number of transitions of these molecules would be important. However, current ground-based telescopes such as the VLT CRIRES+ (Follert et al. 2014) only reach up to 5 μm. Atomic Li lines at 600–900 nm could be detected using CAHA 3.5 CARMENES (520–1710 nm, $R > 80{,}000$; Quirrenbach et al. 2010) and the Subaru/High Dispersion Spectrograph (298–1016 nm, $R > 90{,}000$; Noguchi et al. 2002).

Another potential avenue for fundamental research is to improve the thermodynamic data in order to understand the reason for the apparent nondetection of the Li 670.8 nm line in T dwarf thermal fluxes. Knowing the kinetic data between all Li-bearing reactions, as well as their condensation, would be another topic to advance for future work.

7. Supplementary Data

The pregenerated ACS data of LiH, LiF, and LiCl from this study are publicly available in 10.5281/zenodo.4921928.

We would like to thank Dr. Adam Burgasser for his assistance regarding the observational T dwarf spectra. E.G.N. acknowledges Research Computing at Arizona State University for providing HPC resources that have contributed to the research results reported within this paper. E.G.N. acknowledges support from HST-AR-15796 to generate Li species opacities. We also acknowledge the ExoMol team for their continued production of large line lists and pertinent data critical to high-temperature atmospheric modeling. E.G.N.'s research was supported by an appointment to the NASA

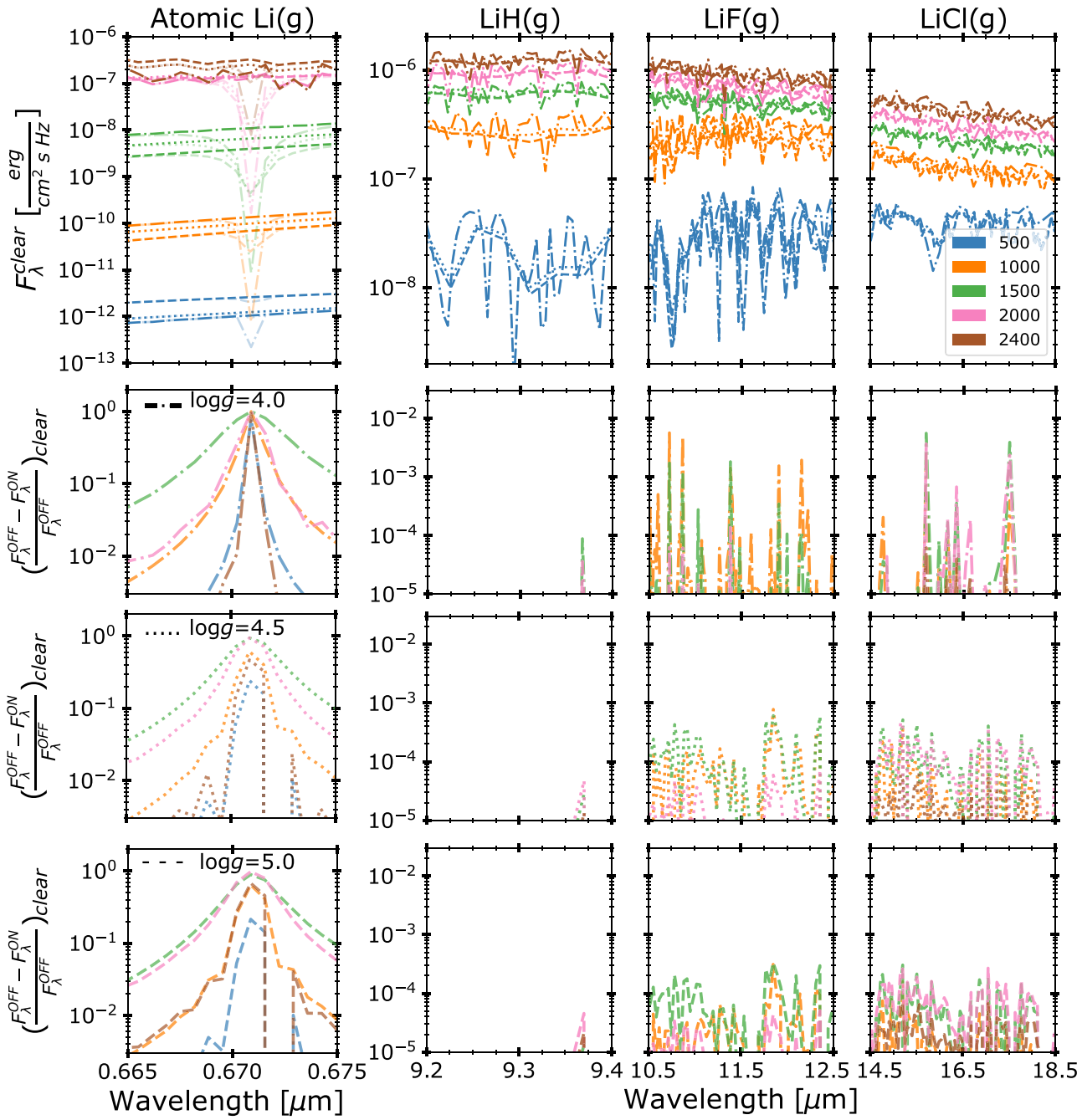

Figure 6. Similar to Figure 5, but for cloudless spectra and different $T_{\rm eff}$ in 500–2400 K range with $\log g = 4.0$ (dashed-dotted), $\log g = 4.5$ (dotted) and 5.0 (dashed). (Top panels) The presence ($F^{\rm ON}$, solid) and absence ($F^{\rm OFF}$, dashed) of Li, LiH, LiF, and LiCl. As with the cloudy model cases, atomic Li shows a noticeable difference between its $F^{\rm ON}$ and $F^{\rm OFF}$ spectra. The bottom three rows show the relative flux ratio, which is the difference between $F^{\rm ON}$ and $F^{\rm OFF}$ normalized by $F_{\rm OFF}$ ($\mathcal{F}_{\rm R} \equiv \frac{F^{\rm OFF}-F^{\rm ON}}{F^{\rm OFF}}$) for $\log g = 4.0$, 4.5 and 5. All spectra are smoothed for clarity. The spectral features of LiF and LiCl are stronger at lower surface gravity. LiH is not sensitive to gravity and its $\mathcal{F}_{\rm R}$ is lower than other Li species. LiF and LiCl are most detectable in dwarfs with $M < 65 M_{\rm J}$ at $T_{\rm eff}$ ranges of 1000–1500 K and 1000–2000 K, respectively. Their absence in the observational spectra would be an indicator of higher mass.

Postdoctoral Program at the NASA Ames Research Center, administered by Universities Space Research Association under contract with NASA.

Software: We used the publicly available *ExoCross* code (Yurchenko et al. 2018) developed by the ExoMol group to generate the cross sections. To perform the radiative transfer modeling of brown dwarfs, the `PICASO` tool was used (Batalha 2019; Batalha et al. 2019). Brown dwarf thermal structures and cloud compositions from `Sonora` cloudless and cloudy models (Marley et al. 2018, 2021) were used.

ORCID iDs

Ehsan Gharib-Nezhad https://orcid.org/0000-0002-4088-7262
Mark S. Marley https://orcid.org/0000-0002-5251-2943
Natasha E. Batalha https://orcid.org/0000-0003-1240-6844

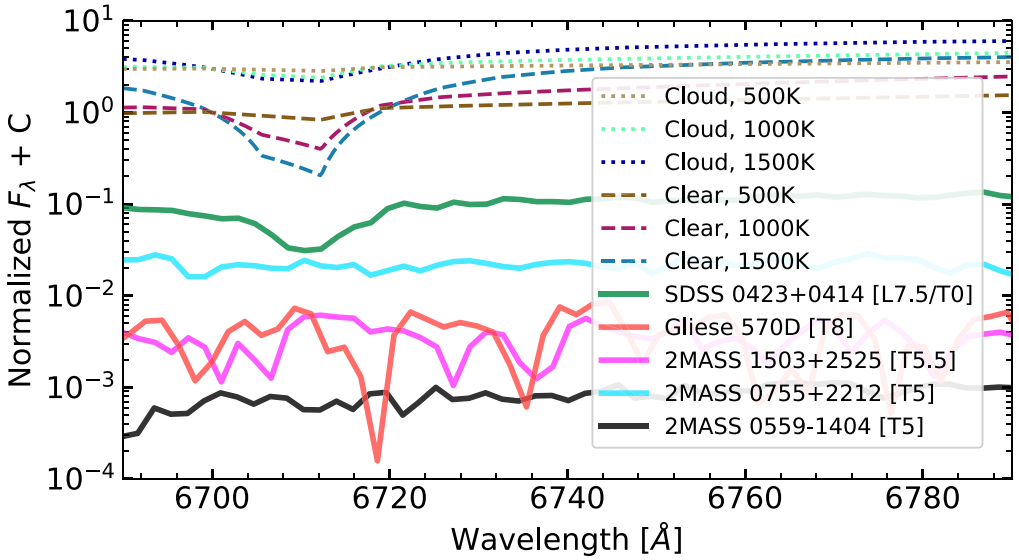

Figure 7. Comparing a set of observed T dwarf fluxes with synthetic spectra from Sonora cloudy and cloud-free models ($\log g = 5$). Theoretical evolution models predict the detection of atomic Li 6708 Å, whereas many T-dwarf spectra have not shown any Li signature. For example, observed fluxes for Gliese 570D, 2MASS 0559-1404, 2MASS 0755+2212, 2MASS 1503+2525 do not show any Li absorption. ‘ Note, the Near-Infrared part of the spectrum is T0, while the optical part of the SDSS 0423-0414 (SDSS J042348.57-041403.5) flux is classified as L7.5 and so it shows the Li line with EW = 11 Å(Kirkpatrick et al. 2008; Vrba et al. 2004) (spectra are from Burgasser et al. 2003a and Kirkpatrick et al. 2008).

Channon Visscher https://orcid.org/0000-0001-6627-6067
Richard S. Freedman https://orcid.org/0000-0001-9333-4306
Roxana E. Lupu https://orcid.org/0000-0003-3444-5908

References

Ackerman, A. S., & Marley, M. S. 2001, ApJ, 556, 872
Allard, F., Hauschildt, P. H., Alexander, D. R., Tamanai, A., & Schweitzer, A. 2001, ApJ, 556, 357
Allard, F., Hauschildt, P. H., Baraffe, I., & Chabrier, G. 1996, ApJL, 465, L123
Allers, K. N., & Liu, M. C. 2013, ApJ, 772, 79
Basri, G. 2000, ARA&A, 38, 485
Batalha, N. 2019, natashabatalha/picaso: Initial Publication Release, v0.0, Zenodo
Batalha, N. E., Marley, M. S., Lewis, N. K., & Fortney, J. J. 2019, ApJ, 878, 70
Bildsten, L., Brown, E. F., Matzner, C. D., & Ushomirsky, G. 1997, ApJ, 482, 442
Bittner, D. M., & Bernath, P. F. 2018, ApJS, 236, 46
Brandt, T. D., Dupuy, T. J., Bowler, B. P., et al. 2020, AJ, 160, 196
Bunker, P. R., Jensen, P., Karpfen, A., & Lischka, H. 1989, JMoSp, 135, 89
Burgasser, A. J., Kirkpatrick, J. D., Liebert, J., & Burrows, A. 2003a, ApJ, 594, 510
Burgasser, A. J., Kirkpatrick, J. D., McElwain, M. W., et al. 2003b, AJ, 125, 850
Burgasser, A. J., Kirkpatrick, J. D., Brown, M. E., et al. 2002, ApJ, 564, 421
Burrows, A., Burgasser, A. J., Kirkpatrick, J. D., et al. 2002, ApJ, 573, 394
Burrows, A., Hubbard, W. B., Lunine, J. I., & Liebert, J. 2001, RvMP, 73, 719
Burrows, A., Marley, M., Hubbard, W. B., et al. 1997, ApJ, 491, 856
Chabrier, G., Baraffe, I., Allard, F., & Hauschildt, P. 2000, ApJ, 542, 464
Chabrier, G., Baraffe, I., & Plez, B. 1996, ApJ, 459, L91
Coppola, C. M., Lodi, L., & Tennyson, J. 2011, MNRAS, 415, 487
Crepp, J. R., Gonzales, E. J., Bechter, E. B., et al. 2016, ApJ, 831, 136
Cushing, M. C., Rayner, J. T., & Vacca, W. D. 2005, ApJ, 623, 1115
Follert, R., Dorn, R. J., Oliva, E., et al. 2014, Proc. SPIE, 9147, 914719
Freedman, R. S., Lustig-Yaeger, J., Fortney, J. J., et al. 2014, ApJS, 214, 25
Geballe, T. R., Saumon, D., Leggett, S. K., et al. 2001, ApJ, 556, 373
Gharib-Nezhad, E., Iyer, A. R., Line, M. R., et al. 2021, ApJS, 254, 34
Kirkpatrick, J. D., Reid, I. N., Liebert, J., et al. 2000, AJ, 120, 447
Kirkpatrick, J. D., Cruz, K. L., Barman, T. S., et al. 2008, ApJ, 689, 1295
Koput, J. 2013, JChPh, 138, 234301
Liu, M. C., Fischer, D. A., Graham, J. R., et al. 2002, ApJ, 571, 519
Lodders, K. 1999, ApJ, 519, 793
Lodders, K. 2003, ApJ, 591, 1220
Lupu, R. E., Zahnle, K., Marley, M. S., et al. 2014, ApJ, 784, 27
Magazzu, A., Martin, E. L., & Rebolo, R. 1993, ApJL, 404, L17
Maire, A. L., Molaverdikhani, K., Desidera, S., et al. 2020, A&A, 639, A47
Marley, M., Saumon, D., Morley, C., & Fortney, J. 2018, Sonora 2018: Cloud-free, solar composition, solar C/O substellar atmosphere models and spectra, Zenodo,
Marley, M. S., & Robinson, T. D. 2015, ARA&A, 53, 279
Marley, M. S., Saumon, D., Guillot, T., et al. 1996, Sci, 272, 1919
Marley, M. S., Saumon, D., Morley, C., et al. 2021, ApJ, at press
Martín, E. L., Basri, G., & Zapatero Osorio, M. R. 1999, AJ, 118, 1005
Martín, E. L., Lodieu, N., Pavlenko, Y., & Béjar, V. J. S. 2018, ApJ, 856, 40
McGovern, M. R., Kirkpatrick, J. D., McLean, I. S., et al. 2004, ApJ, 600, 1020
Nakajima, T., Oppenheimer, B. R., Kulkarni, S. R., et al. 1995, Natur, 378, 463
Nelson, L. A., Rappaport, S., & Chiang, E. 1993, ApJ, 413, 364
Noguchi, K., Aoki, W., Kawanomoto, S., et al. 2002, PASJ, 54, 855
Oppenheimer, B. R., Kulkarni, S. R., Matthews, K., & Nakajima, T. 1995, Sci, 270, 1478
Pavlenko, Y. V., Jones, H. R. A., Martín, E. L., et al. 2007, MNRAS, 380, 1285
Pozio, F. 1991, MmSAI, 62, 171
Quirrenbach, A., Amado, P. J., Mandel, H., et al. 2010, Proc. SPIE, 7735, 773513
Rebolo, R., Martin, E. L., Basri, G., Marcy, G. W., & Zapatero-Osorio, M. R. 1996, ApJL, 469, L53
Rebolo, R., Martin, E. L., & Magazzu, A. 1992, ApJL, 389, L83
Rebolo, R., Zapatero Osorio, M. R., & Martín, E. L. 1995, Natur, 377, 129
Sahlmann, J., Burgasser, A. J., Bardalez Gagliuffi, D. C., et al. 2020, MNRAS, 495, 1136
Saumon, D., & Marley, M. S. 2008, ApJ, 689, 1327
Vrba, F. J., Henden, A. A., Luginbuhl, C. B., et al. 2004, AJ, 127, 2948
Weck, P. F., Schweitzer, A., Kirby, K., Hauschildt, P. H., & Stancil, P. C. 2004, ApJ, 613, 567
Yurchenko, S. N., Al-Refaie, A. F., & Tennyson, J. 2018, A&A, 614, A131
Zhang, X. 2020, RAA, 20, 099